INTERNATIONAL JOURNAL FOR NUMERICAL METHODS IN FLUIDS
Int. J. Numer. Meth. Fluids 2004; **45**:797–817 (DOI: 10.1002/fld.724)

A convection–diffusion CFD model for aeolian particle transport

S. B. Ji, A. G. Gerber*,† and A. C. M. Sousa

Department of Mechanical Engineering, University of New Brunswick, P.O. Box 4400, Fredericton, NB., Canada E3B-5A3

SUMMARY

A convection–diffusion mixture model for estimating particle transport along loose surfaces, which can be incorporated within the framework of a computational-fluid-dynamics (CFD) solution, is presented. In consideration of the particle behaviour of saltation and suspension in wind tunnel tests, the particle flow is described by the basic parameters controlled by the surface shear stress and particle size. This description is used to derive a surface entrainment rate, and effective near-wall saltation diffusion coefficient applied in mixture models of two-phase flow. The derivation leads to equations that provide, based on a specified surface shear stress and particle size, an appropriately scaled estimation of the particle entrainment into the flow. Validation has been conducted against air–sand and air–coal systems where experimental and numerical predictions are available for comparison. Copyright © 2004 John Wiley & Sons, Ltd.

KEY WORDS: sediment transport; loose boundaries; computational fluid dynamics (CFD); turbulence

INTRODUCTION

Aeolian saltation on a loose boundary is a common occurrence in nature and in many industrial processes. Often there is interest in estimating the amount of material entrained from the loose surface, and the degree to which it is transported within the carrier fluid. Such estimations are difficult due to the complex interaction of the entrained particles with a, normally, turbulent flow field, and the particle–particle interactions at the surface. Since the airflow is rarely fully developed along the surface, and particles generally have a wide distribution in size, the ability to estimate entrainment rates is severely limited by using semi-analytical methods alone. Well-established experiments to measure entrainment rates, and to determine

*Correspondence to: A. G. Gerber, Department of Mechanical Engineering, University of New Brunswick, P.O. Box 4400, Fredericton, NB., Canada E3B-5A3.
†E-mail: agerber@unb.ca

Contract/grant sponsor: University of New Brunswick
Contract/grant sponsor: Natural Sciences and Engineering Research Council of Canada

Published online 4 May 2004

Received 3 April 2003
Revised 18 February 2004

particle statistics have been performed, but these controlled wind tunnel flows are considerably simplified relative to practical situations. To obtain entrainment estimations in more practical flow situations, computational-fluid-dynamics (CFD) can be employed to provide a good prediction on the near surface flow conditions. However, as yet, no methodology exists to incorporate material entrainment over a loose surface into a CFD model of sediment transport, that reflects experimentally observed particle transport behaviour in such conditions.

The present paper describes an approach for introducing sediment transport over loose surfaces into a CFD solution. The derivation approach applies the general characteristics of sediment transport behaviour along loose surfaces, where these characteristics have been observed by a large number of researchers both by experiment and computation [1–11]. These characteristics will be discussed in detail subsequently.

Computational models of sediment transport have been attempted by a number of researchers. For the most part these models focus on the dynamics of individual particles near the surface, and by solving a large number of particles, each with different starting conditions, a statistical estimate of the transport behaviour near a surface can be obtained. These models usually include the surface saltation processes of particle aerodynamic entrainment, surface impact and rebound, ejection, and gravitational settling [3–6]. These calculations reflect the experiments, which are for well-controlled fully developed flow conditions. Since particles are tracked in a large number, these computational methods are not generally practical for large-scale flows. Researchers have employed continuum solutions to sediment transport using CFD [12–14], however no clear method has been presented for applying surface entrainment rates into the solution, instead the emphasis has been placed on the algorithm development for moving boundaries.

DESCRIPTION OF NEAR SURFACE SEDIMENT TRANSPORT

Beginning with the early research of Bagnold [1], up to more recent experimental and computational studies [7, 10, 11], loose surface transport has been described by two processes known as suspension and saltation. Suspension occurs primarily with small particle sizes ($<100\,\mu\text{m}$) where turbulent mixing in the carrier fluid is sufficient to keep the particles suspended and away from the surface. Saltation, however dominates at larger particle sizes, and involves particle impact at the surface, its rebound and the ejection of other particles. Due to the larger sizes gravitational settling is always present to keep the particles from remaining permanently airborne. Saltation involves a dynamic balance between particles entrained by surface aerodynamic forces, rebounding or ejection into the free-stream and particles returning to the surface by settling. The distinction between suspension and saltation is clear at the smaller and larger particle sizes, but at intermediate sizes there is no clear distinction as both processes are active.

Experimental work has shown that the vertical particle flux profile, $f(y)$, along a flat saltating surface, can be described by an exponential function of the form [6]

$$f(y) \approx f(0)\exp(-\lambda_m y/\delta) \tag{1}$$

where $f(0)$ is the flux at the surface, λ_m is a dimensionless parameter, and δ a vertical scaling parameter based on the surface shear stress. The above flux profile is well established,

in particular far away from threshold conditions, and likewise the total horizontal particle flux per unit span has been found to follow:

$$F \approx C_s \rho u_*^3 / g \tag{2}$$

where u_* is the surface shear velocity ($= \sqrt{\tau_w/\rho}$), ρ the fluid density, and C_s a constant dependent on particle size.

The primary scaling parameter in the saltation layer is the surface shear velocity. This measures the strength of the surface shear stress, which is the primary mechanism for initiating saltation (and suspension) and for delivering energy to the surface to sustain the saltation process. A typical scaling parameter would be $\delta = (k_0 u_*)^2/g$, which estimates the thickness of the saltation layer if an appropriate value for k_0 is utilized from experiments.

The present paper describes a model for saltation and suspension that incorporates the fundamental behaviour of particles embodied in Equations (1) and (2). Therefore, in the case of simple duct flow, for which the experiments are most analogous, the model closely recovers the results obtained by many researchers. In the context of a more general fluid flow situation, for which CFD is most useful, the proposed saltation and suspension model provides a good first-order estimate of the entrainment fluxes, and as a result an improved estimation of the motion and dispersion of the particles.

MULTIPHASE FLOW MODEL FOR SUSPENSION AND SALTATION

Multiphase flows can be modelled using a wide variety of approaches, each approach suited for a particular combination of assumptions (for example no interphase slip or heat transfer) and/or level of detail required from the analysis. In the present case the interest is in the larger scale transport of sediment (i.e. much larger than the size scale of the particles), and not the detailed fluid/particle interactions. For the conditions typical of saltation and suspension, the two-phase flow can be classified as dilute so that particle–particle collisions are few. A wide range of particle sizes may be present and the computational procedure should be efficient to handle such cases. In some cases the surface deformation, resulting from aggressive entrainment of surface material, becomes significant enough that it must be included in the computations. To meet these requirements a CFD multiphase model based on the well-established algebraic-slip approximation can be applied along with a moving grid scheme to accommodate deforming boundaries [12]. Since the focus of the present work is the entrainment fluxes at the surface, results for surface deformation will not be included.

A CFD simulation based on the algebraic-slip approximation utilizes only a single-set of momentum equations to model the bulk motion of the fluid mixture. The slip of the dispersed phase, relative to the bulk motion, is modelled through an algebraic model. This algebraically defined slip is applied to the conservation equations for the dispersed phase, which might be comprised of several particle groups. The system of equations, shown in tensor notation, for the general case of three-dimensional incompressible turbulent flow with n particle sizes is

$$\frac{\partial \rho u_j}{\partial x_j} = 0 \tag{3}$$

$$\frac{\partial \rho u_i}{\partial t} + \frac{\partial \rho u_j u_i}{\partial x_j} = \frac{\partial}{\partial x_j}\left(\mu_{\text{eff}} \frac{\partial u_i}{\partial x_j}\right) - \frac{\partial p}{\partial x_i} + F_i \tag{4}$$

$$\frac{\partial \rho \phi_n}{\partial t} + \frac{\partial \rho u_j \phi_n}{\partial x_j} = \frac{\partial}{\partial x_j}\left(\Gamma_{\text{eff}} \frac{\partial \phi_n}{\partial x_j}\right) - \frac{\partial \rho v_{sj} \phi_n}{\partial x_j} \tag{5}$$

Note that Equation (5) represents only one of n possible particle sizes, and that the last term on the right-hand side is the algebraic slip contribution. The physical properties for all of the equations are those of the continuous phase. The coefficient F_i accounts for the smaller contributions of the viscous stress tensor.

Since most practical flows are turbulent, a turbulence model is also required. Considering the assumptions made, it is reasonable to select the k–ε model—the most widely used RANS (Reynolds-averaged Navier–Stokes equations) turbulence model. Wall shear stresses are estimated by resorting to wall functions. This model is used for the CFD application to be described later on, and since the solid phase is dilute in much of the gas phase only one-way coupling is considered. The turbulent viscosity, μ_t, is computed from a velocity scale ($V_t = k^{1/2}$) and a length scale ($l_t = k^{3/2}/\varepsilon$) predicted at each point in the flow via the solution of transport equations for k and ε. The turbulent viscosity then becomes

$$\mu_t = \rho C_\mu l_t V_t = \rho C_\mu \frac{k^2}{\varepsilon} \tag{6}$$

Local value of k and ε are obtained from the solution of the following semi-empirical transport equation:

$$\frac{\partial(\rho k)}{\partial t} + \frac{\partial(\rho u_j k)}{\partial x_j} = \frac{\partial}{\partial x_j}\left(\Gamma_k \frac{\partial k}{\partial x_j}\right) + P_k - \rho\varepsilon \tag{7}$$

$$\frac{\partial(\rho \varepsilon)}{\partial t} + \frac{\partial(\rho u_j \varepsilon)}{\partial x_j} = \frac{\partial}{\partial x_j}\left(\Gamma_\varepsilon \frac{\partial \varepsilon}{\partial x_j}\right) + \frac{\varepsilon}{k}(C_{\varepsilon 1} P_k - \rho C_{\varepsilon 2} \varepsilon) \tag{8}$$

A complete description of the k–ε model can be found in Reference [15].

To successfully apply Equations (3)–(8) to saltation and suspension, several modifications to Equation (5) are required, namely

1. The effective diffusion coefficient, Γ_{eff}, should include an additional term to account for the saltation activity near a loose boundary.
2. Entrainment fluxes, along a loose boundary, which are a function of surface flow conditions, need to be modelled.
3. In the context of a convection–diffusion CFD model, the saltation influence along the loose boundary must be scaled relative to the size of the saltation layer thickness.

In subsequent sections, each of these modifications are described. However, first the mechanisms for surface entrainment, and the evaluation of the settling velocity required in the algebraic slip assumption, need to be formulated.

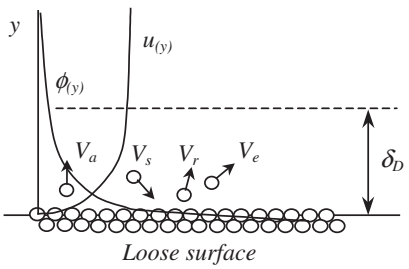

Figure 1. Loose surface conditions, within saltation layer thickness δ_D, with particle actions by aerodynamic entrainment (at velocity V_a), settling to surface (V_s), rebound from impact (V_r), and ejection from impact (V_e).

Surface entrainment

Particles are entrained into the fluid if a threshold condition along the surface is reached. The threshold is based on the definition of a critical 'surface' shear stress, τ_0, where the 'surface' is a loose layer of sand as shown in Figure 1. The threshold condition proposed in [3, 16] is utilized in this study, and it assumes that if exceeded, then aerodynamic forces are large enough to expel a particle into the moving fluid. The threshold increases with particle diameter since, with a larger body force, the particle should be more difficult to dislodge from the surface.

The threshold determines when a particle should be released into the fluid stream, and the rate at which the particles are removed from the surface depends on the relation

$$\dot{N} m_p = \max(\zeta(\tau - \tau_0), 0) \tag{9}$$

which models the removal rate as linear with respect to the excess shear past threshold. In Equation (9), $\dot{N}$ is the particle number flux at the surface and ζ the entrainment coefficient for a given particle size (m_p is the particle mass). In Figure 1 is shown the action of particles aerodynamically entrained (at velocity V_a), settling toward the surface (V_s), rebounding after impact (V_r), and ejected by impact (V_e). In the present paper, Equation (9) is used to represent the net entrainment into the flow, and therefore also includes particle entrainment by rebound and ejection. The settling influence is embedded in terms of settling velocity.

Settling velocity

A competing surface action is the return of particles to the surface. This settling effect is incorporated into the model through the algebraic-slip contribution to Equation (5). At the surface the net effect of entrainment and settling determines the rate at which the surface deforms. At steady-state the two effects counter-balance so that no net particles are entrained into the flow.

Particles entrained into the flow will eventually return to the surface if the particle size is large. The descent of a particle in a turbulent flow field is assumed to have on average no slip in the horizontal direction with an average vertical slip equal to the fall (or terminal) velocity, v_s, of the particle. It is well known that particles settle back toward the surface at a speed very close to their terminal velocity [16]. This terminal or fall velocity is calculated

assuming equilibrium conditions between the downward (in the direction of gravity) particle body-force and the upward drag force between fluid and particle. The resulting equation is

$$v_s = \sqrt{\frac{4}{3}\frac{(\rho_p - \rho)gd}{C_D\rho}} \tag{10}$$

where the drag coefficient depends on the particle size. In this work a drag law proposed by Schiller and Naumann [17] is used

$$C_D = \frac{24}{Re}(1 + 0.15\,Re^{0.687}) \tag{11}$$

which is appropriate for particle Reynolds numbers smaller than 800. Equations (10) and (11) must be solved iteratively to obtain the settling velocity associated with a given particle size.

ESTIMATION OF EFFECTIVE DIFFUSIVITY COEFFICIENT (Γ_{eff})

The derivation of the effective diffusion coefficient to be employed in Equation (5) begins by considering the transport conditions, for a specific particle size, in a two-dimensional fully developed (or steady-state) saltation layer. With fully developed flow all gradients in the flow direction become zero ($\partial\phi_n/\partial x = 0$) and the vertical velocity, v, is small compared to the horizontal and settling velocity ($v \ll u$ and $v \ll v_s$). The resulting transport equation includes diffusive mixing, and a slip velocity v_s representing the particle gravitational settling. This is shown as

$$\Gamma_{eff}\frac{\partial^2\phi_n}{\partial y^2} - \rho v_s\frac{\partial\phi_n}{\partial y} = 0 \tag{12}$$

which is a second-order differential equation where, assuming the diffusion coefficient, Γ_{eff}, can be approximated as uniform over the saltation layer, the solution is straightforward

$$\phi_n(y) = Ce^{(\rho v_s/\Gamma_{eff})y} \quad \text{or} \quad \ln\,\phi_n(y) = \ln\,C + \frac{\rho v_s}{\Gamma_{eff}}\,y \tag{13}$$

It should be emphasized that this result applies only to a given particle size n. In Figure 2 the log profile of ϕ_n is plotted versus distance y from the surface. The extent of the saltation/suspension layer can be approximated by the intersection of the line with the horizontal axis at D. The slope is negative because the slip velocity, v_s, is defined as negative based on the direction of gravity (towards the surface). The gradient of $\ln\,\phi_n(y)$ depends on the relative strength of the effective diffusivity and slip velocity, and represents the competitive actions of turbulent diffusion (which also embodies diffusive-like saltation mechanisms to be described later) away from the surface and settling processes toward the surface.

The constant C can be estimated with the value of $\phi_n(y)$ at the surface ($\phi_n(0) = C = \phi_S$). The value of ϕ_n at the surface can be determined at fully developed steady-state conditions by conserving the settling and entrainment fluxes at the surfaces so that

$$\zeta(\tau_w - \tau_0) + \rho v_s\phi_S = 0 \tag{14}$$

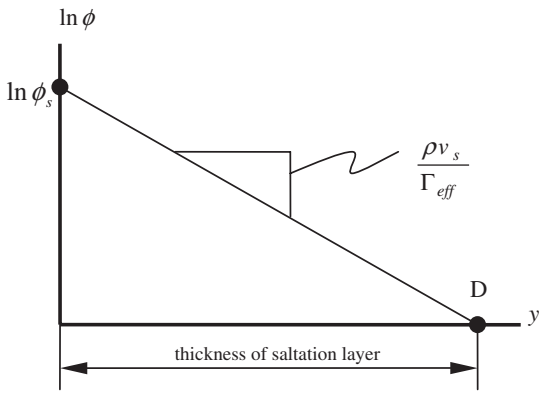

Figure 2. Particle concentration profile through saltation layer.

This equation can be re-arranged to give

$$\phi_{\mathrm{S}} = \frac{-\zeta(\tau_{\mathrm{w}} - \tau_0)}{\rho v_{\mathrm{s}}} \tag{15}$$

With this result the final form for function $\phi_n(y)$ becomes

$$\phi_n(y) = \frac{\zeta(\tau_{\mathrm{w}} - \tau_0)}{-\rho v_{\mathrm{s}}} \, \mathrm{e}^{(\rho v_{\mathrm{s}}/\Gamma_{\mathrm{eff}})y} \tag{16}$$

Generally, in many experiments, these log profiles are given as mass fluxes as indicated by Equation (1). For direct comparison to experiment, Equation (16) must be multiplied by the velocity profile near the sand surface, which, as an initial estimate, can be the standard log-law profile

$$u(y) = \frac{u_*}{\kappa} \ln\left(\frac{u_* y}{\nu}\right) + u_* B \tag{17}$$

so that Equation (16) becomes

$$\dot{m}_{\mathrm{p}}(y) = \rho u(y)\phi(y) = \rho \left[\frac{u_*}{\kappa} \ln\left(\frac{u_* y}{\nu}\right) + u_* B\right] \left[\frac{\zeta(\tau_{\mathrm{w}} - \tau_0)}{-\rho v_{\mathrm{s}}}\right] \mathrm{e}^{(\rho v_{\mathrm{s}}/\Gamma_{\mathrm{eff}})y} \tag{18}$$

where κ and B are taken to be equal to 0.41 and 5.0, respectively.

Equation (18) has only two adjustable constants, the entrainment coefficient ζ and the effective diffusivity Γ_{eff}. To provide a complete analytical description for the problem, a procedure to determine ζ and the effective diffusivity Γ_{eff} as functions of particle diameter and surface shear velocity is required.

This simplified analytical model suggests two important features: (i) the effective diffusivity is enhanced up to the surface in the saltation layer, and reflects the increasing influence of saltation activity near the surface (this is contrary to the trend for the effective diffusivity due to turbulence, which tends zero at the surface), and (ii) it is possible to use a convection–diffusion scalar equation, with an algebraic definition of slip, to approximate the processes of saltation and suspension. It should be noted that in modelling saltation/suspension in this

manner, the effective diffusivity definition, generally modelled as having only molecular and turbulent contributions, should also include a term for surface saltation. In this case Γ_{eff} can be defined in a simplified form as

$$\Gamma_{\text{eff}} = \Gamma_{\text{m}} + \Gamma_{\text{s}} + \frac{\mu_{\text{t}}}{\sigma_{\text{d}}} \tag{19}$$

where Γ_{s} is a diffusion coefficient to represent the increasing saltation influence near the loose surface. An equation for Γ_{s} will be discussed subsequently.

To obtain Γ_{eff} one can utilize a typical length scale, δ_{D}, for the saltation layer thickness (which is estimated using experimental data) in conjunction with Figure 2. Based on a number of researchers [2, 3, 6] the saltation layer height, δ_{D}, scales with the square of the shear velocity times a constant k_0, so that

$$\delta_{\text{D}} = \frac{(k_0 u_*)^2}{2g} \tag{20}$$

The parameter k_0 is obtained from experimental studies, and has been found to consistently range between 1 and 2. The value of k_0 has also been discussed by Nalpanis *et al.* [6] to have a particle size dependence and, in this work, has been replaced by a general form

$$k_0 = 1 + A\left(1 - \frac{d}{d_1}\right) \tag{21}$$

where, based on the studies of Anderson and Haff [3] and Nalpanis *et al.* [6], $d_1 = 250\ \mu\text{m}$ and $A = 1.673$.

Equation (20) can be used to estimate the saltation layer thickness y_{D} so that based on Figure 2 Γ_{eff} can be estimated as

$$\Gamma_{\text{eff}} = \frac{\delta_{\text{D}} \rho v_{\text{s}}}{\ln(\phi_\infty / \phi_{\text{s}})} \tag{22}$$

where the denominator is the ratio of the free-stream dust concentration level to that near the surface. Using the fluid boundary layer analogy, this ratio can be defined at $\phi_\infty = 0.01\ \phi_{\text{s}}$ so that Equation (22) becomes

$$\Gamma_{\text{eff}} = \beta \delta_{\text{D}} \rho v_{\text{s}} \tag{23}$$

where $\beta = -0.217$. With k_0 taken from experimental studies, the value for Γ_{eff} can be calculated knowing the particle size and wall shear velocity in the form

$$\Gamma_{\text{eff}} = \beta \rho k_0^2 u_*^2 v_{\text{s}} / (2g) \tag{24}$$

ESTIMATION OF ENTRAINMENT COEFFICIENT (ζ)

The other important parameter to be determined is the entrainment coefficient (ζ), which represents the net entrainment of material from a loose surface when multiplied by the surface shear stress Equation (9). This includes aerodynamic entrainment of particles, particle rebound,

and particle ejection. Using the total surface flux relation, as given by Equation (2), this coefficient can be estimated. Starting with the equation for total particle entrainment

$$\dot{Q}_{\mathrm{p}} = C_s \frac{\rho}{g} u_*^3 \tag{25}$$

and in order to derive the function ζ, Equation (25) is equated to the integral of Equation (18) over the saltation layer height so that

$$\begin{aligned}\dot{Q}_{\mathrm{p}} &= \int_0^{\delta_{\mathrm{D}}} \dot{m}_{\mathrm{p}}(y)\,\mathrm{d}y = \int_0^{\delta_{\mathrm{D}}} \rho u(y)\phi(y)\,\mathrm{d}y \\ &= \int_0^{\delta_{\mathrm{D}}} \left[\frac{u_*}{\kappa}\ln\left(\frac{u_* y}{\nu}\right) + u_* B\right]\left[\frac{\zeta(\tau_{\mathrm{w}}-\tau_0)}{-v_{\mathrm{s}}}\right] \mathrm{e}^{(\rho v_{\mathrm{s}}/\Gamma_{\mathrm{eff}})y}\,\mathrm{d}y\end{aligned} \tag{26}$$

where the entrainment coefficient can then be calculated by

$$\zeta = \frac{\dot{Q}_{\mathrm{p}}}{\dfrac{(\tau_{\mathrm{w}}-\tau_0)}{-v_{\mathrm{s}}}\displaystyle\int_0^{\delta_{\mathrm{D}}}\left(\frac{u_*}{k}\ln\frac{u_* y}{\nu} + u_* B\right)\mathrm{e}^{\rho v_{\mathrm{s}}/\Gamma_{\mathrm{eff}}\, y}\,\mathrm{d}y} \tag{27}$$

Integration over the saltation layer thickness results in an equation of the form

$$\zeta = \frac{\dot{Q}_{\mathrm{p}}}{(\tau_0-\tau_{\mathrm{w}})(\Gamma_{\mathrm{eff}}/\rho v_{\mathrm{s}}^2)u_*\Pi(u(\delta_{\mathrm{D}})/u_*)} = \frac{C_s(\rho u_* v_{\mathrm{s}})^2}{g(\tau_0-\tau_{\mathrm{w}})\Gamma_{\mathrm{eff}}\Pi(u(\delta_{\mathrm{D}})/u_*)} \tag{28}$$

where the function Π is defined as

$$\Pi(u(\delta_{\mathrm{D}})/u_*) = (\mathrm{e}^{1/\beta}-1)\left(\frac{1}{k}\ln\frac{u_*\delta_{\mathrm{D}}}{\nu} + B\right) - \frac{1}{k}\left(\frac{1}{\beta} + \frac{1}{(2\beta)^2}\right) = C_0(\beta)\frac{u(\delta_{\mathrm{D}})}{u_*} + C_1(\beta) \tag{29}$$

and C_0 and C_1 are the constants since they depend only on the constant β. After expanding γ_{eff}, the final expression for ζ becomes

$$\zeta = \frac{C_s\rho v_{\mathrm{s}}(d)}{\beta k_0^2(\tau_0-\tau_{\mathrm{w}})\Pi(u(\delta_{\mathrm{D}})/u_*)} \tag{30}$$

The function Π evaluates the log-law dimensionless velocity profile at the saltation layer height of δ_{D} with adjustments using C_0 and C_1. In addition also to Γ_{eff}, ζ, is completely defined by the particle diameter and the surface shear velocity. The particle flux-profile, $\dot{m}_{\mathrm{p}}(y)$, as given by Equation (18), is now fully described by the surface shear velocity and particle diameter.

ESTIMATION OF SALTATION DIFFUSIVITY CONTRIBUTION (Γ_{s})

Applying a convection–diffusion model of saltation and suspension to practical three-dimensional flows requires that the near wall diffusion behaviour, embodied in Equations (19) and (24) includes an equation for the saltation diffusion coefficient, Γ_{s}, as a function

of the near wall distance. On the premise that a turbulence model will be employed with Reynolds averaged equations, the Prandtl mixing length model can be used

$$\tau_{xy} = -\overline{u'v'} = \nu_T \frac{\partial U}{\partial y} \tag{31}$$

where ν_T is the kinematic eddy viscosity given by

$$\nu_T = l_{mix}^2 \left| \frac{\partial U}{\partial y} \right| \tag{32}$$

This can be employed for the estimation of the saltation diffusion influence. In the log layer of an incompressible, constant pressure boundary layer, the sum of the viscous and Reynolds shear stress is approximately constant and equal to the wall shear stress

$$\nu \frac{\partial U}{\partial y} - \overline{u'v'} \approx \nu \left(\frac{\partial U}{\partial y} \right)_{wall} = \frac{\tau_w}{\rho} = u_*^2 \tag{33}$$

which is used to derive the log layer velocity profile, Equation (17) on the basis of the turbulence length scale

$$l_{mix} = ky \tag{34}$$

Using this length scale to obtain the dynamic eddy viscosity from Equation (32) we have

$$\mu_t = k\rho u_* y \tag{35}$$

The use of a more detailed mixing length formula proposed by Cebeci and Smith [18] led only to minor changes for the purposes of Γ_s estimation. In the interest of a straightforward implementation, the simplest mixing length model was used (Equation (34)).

With the value of Γ_{eff} known from Equation (24), and Γ_t, from Equation (35) (when divided by the turbulent Prandtl number, σ_d), and assuming the molecular diffusion is small ($\Gamma_m = 0$) the saltation diffusion contribution can be written as

$$\Gamma_s = \beta \rho v_s \delta_D - \frac{k\rho u_* y}{\sigma_d} \tag{36}$$

where σ_d is the turbulent Prandtl number for the dispersed phase. In this relation the saltation diffusivity coefficient must have a value 0 at the outer edge of the saltation layer (i.e. $\Gamma_s = 0$ ($y = \delta_D$)). This allows the turbulent Prandtl number to be estimated in the saltation layer as a function of the wall shear velocity. For example $\sigma_d = 0.486$ for a flow with $u_* = 0.35$ (and particle diameter of 188 μm) which is close to values generally used (ranging from 0.1 to 1) in practice for scalar transport equations. In general for the saltation case

$$\sigma_d = \frac{k}{\beta} \frac{u_*}{v_s} \tag{37}$$

so that Equation (36) can be rewritten as

$$\Gamma_s = \mathrm{Max}(\beta \rho v_s (\delta_D - y), 0) \tag{38}$$

Equation (38) can be applied along loose boundaries in particle transport using convection–diffusion equations in conjunction with the definition for Γ_{eff} as given in Equation (19).

In summary Equations (19), (30) and (38) can be utilized in a CFD simulation where loose boundaries are prevalent. The solution will recover the saltation/suspension behaviour typical of fully developed flows over flat surfaces, and provides an estimate of entrainment rates in more complex flow situations, if locally fully developed flow is assumed.

DISCUSSION OF EFFECTIVE DIFFUSIVITY AND ENTRAINMENT

The dependence of the derived equations for surface entrainment and diffusivity on u_* and d is explored in this section. From Figure 3, it can be seen that, for the range of particle sizes shown, the entrainment coefficient increases with a decrease in shear velocity. The entrainment coefficient also increases rapidly with particle size, at reduced shear velocities. This behaviour can be understood when noting that the definition of ζ incorporates not only aerodynamic entrainment, but also ejection and rebound. As the saltation layer thins (at reduced u_* and increased d), particle trajectories are compacted toward the surface. A rebounding particle visits the surface more frequently and this increased surface activity is reflected in the entrainment coefficient response. At very low u_*, threshold conditions are not reached and entrainment ceases from the surface. The threshold curve (laminar limit) is also shown in Figure 3. Associated with the entrainment coefficient is the total entrainment from the surface as a function of u_* and d as shown in Figure 4. In this case total entrainment is relatively insensitive to u_* but strongly dependent on particle size. While the amount of material removed from the surface, at a fixed diameter, remains relatively constant, the energy imparted to the removed particles is increased with u_*. This results in a substantial growth in the saltation layer height (particles have much higher and longer trajectories) as shown by the saltation layer curve (at one fixed diameter) in Figure 4. A larger saltation layer carries more particles horizontally over the surface so that the total amount of material entrained is increased in accordance with Equation (2). The significant influence of particle size on total entrainment is due to the larger

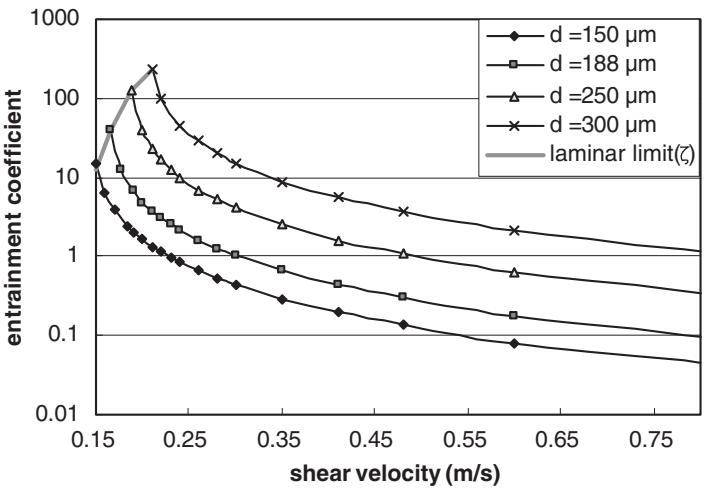

Figure 3. Functional dependence of entrainment coefficient: $\zeta = f(d, u_*)$.

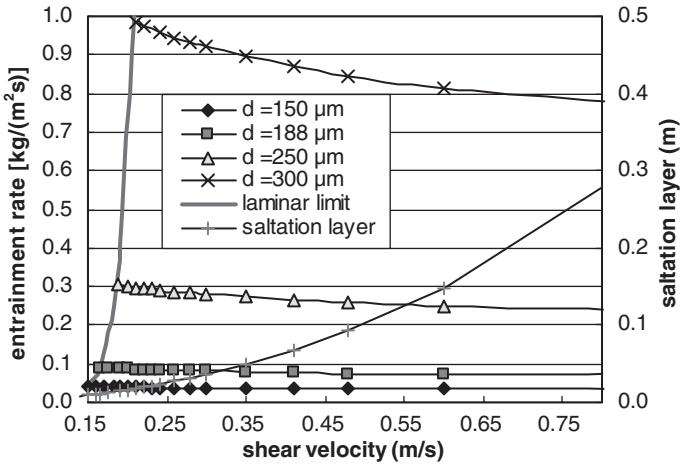

Figure 4. Total entrainment rate over loose surface ($=\zeta(\tau_w - \tau_0)$) and saltation layer thickness for $d = 188$ μm.

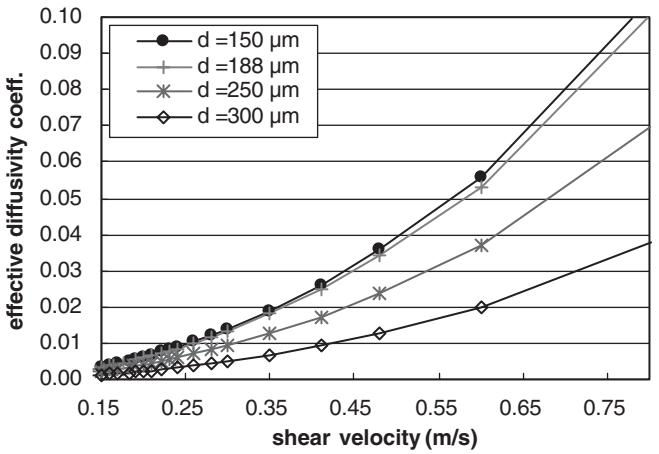

Figure 5. Functional dependence of effective diffusivity coefficient: $\Gamma_{\text{eff}} = f(d, u_*)$.

mass contained in larger particles. Larger particles also decrease the saltation layer thickness so that rebound and ejection activity at the surface, in a manner similar to that discussed for the entrainment coefficient in Figure 3, is increased.

The behaviour of the effective diffusivity coefficient, shown in Figure 5, also needs to be explained. In this case the trend is an increase with increasing shear velocity and decreasing particle diameter. While the entrainment coefficient influences the rate at which particles leave the surface, the effective diffusivity coefficient controls the rate at which particles are transported away from the surface towards the free-stream. This process competes with the settling motion back toward the surface (embodied in ρv_s), the net effect being the gradient in

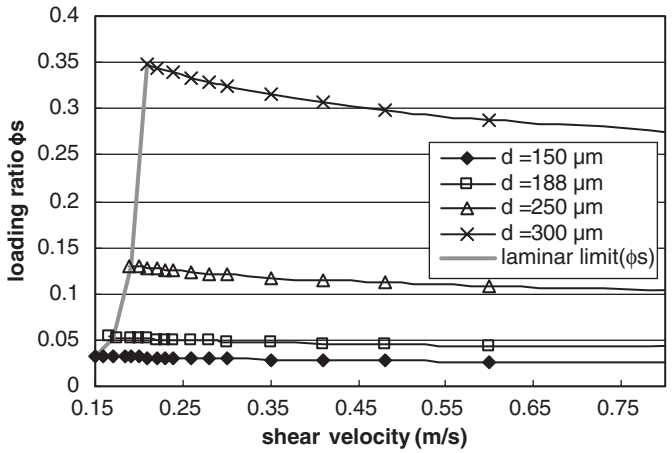

Figure 6. Surface particle concentration (loading ratio) ϕ_s (from Equation (15)) where $\phi_s = f(d, u_*)$.

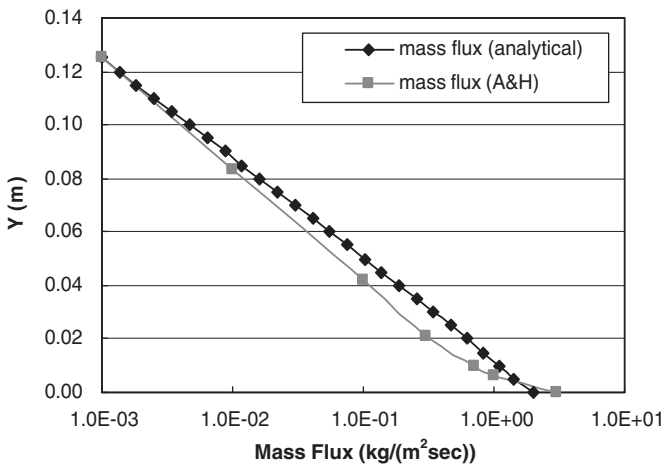

Figure 7. Comparison of analytical model with computational result of Anderson and Haff [3]: $d = 250\,\mu\text{m}$, $u_* = 0.6\,\text{m/s}$.

the flux profile, i.e. the slope shown in Figure 2. The effective diffusion coefficient therefore increases with shear velocity in order to increase the movement of particles away from the surface by increasing the size of the saltation layer. The effective diffusion coefficient becomes smaller with increasing particle size to produce a smaller saltation layer. While the saltation layer gets smaller with larger particle, the increased activity at the surface leads to a larger surface concentration as shown in Figure 6.

The analytical model parameters just described are applied with Equation (18) to the numerical predictions of Anderson and Haff [3] as shown in Figure 7. As can be seen the analytical result represents the average particle behaviour reasonably well. The results for

Anderson and Haff were obtained for conditions in a long duct with a loose boundary, a scenario very similar to the saltation boundary layer analysis described so far.

APPLICATION OF EQUATIONS TO CFD MODEL

A CFD model was developed for two-dimensional flow in a channel, a situation representative of wind tunnel geometries used in saltation/suspension experiments. The bottom surface is modelled as loose through the application of the entrainment equation (Equation (30)), and a near wall saltation influence embodied in Equation (38). The duct is modelled as very long so that fully developed conditions are reached. Various grid resolutions were used to test the sensitivity of the solution to grid refinement. The fully developed results are shown in comparison to experimental data [6] obtained with a particle size of 188 μm, and as shown in Figure 8, the solution with refinement approaches that of experiment for the case of surface shear velocity of 0.35 m/s. In Figure 9 is shown the predictions at five wall shear velocities, with comparison to three cases from experiment. The model trends represent the experimental data well, although at the low shear velocities threshold conditions begin to effect the log profiles of the experimental particle flux. In the vicinity of threshold, the particle entrainment becomes intermittent, which is difficult to model due to the randomness. Numerical results obtained by Nalpanis *et al.* [6], for the same conditions indicate a similar trend, and they are not able to predict near threshold activity. Very importantly, the model predicts the total particle entrainment as a function of near surface shear velocity very well, as seen in Figure 10 in comparison with the same experimental data.

For implementation into a CFD model it is important to discuss the near surface influence of the saltation layer, in comparison with turbulent and molecular diffusion processes also active. In Figure 11 is shown the individual components of the effective diffusivity coefficient, Γ_{eff}, for the CFD solution with $u_* = 0.35$. The molecular diffusivity coefficient, Γ_{m}, is very

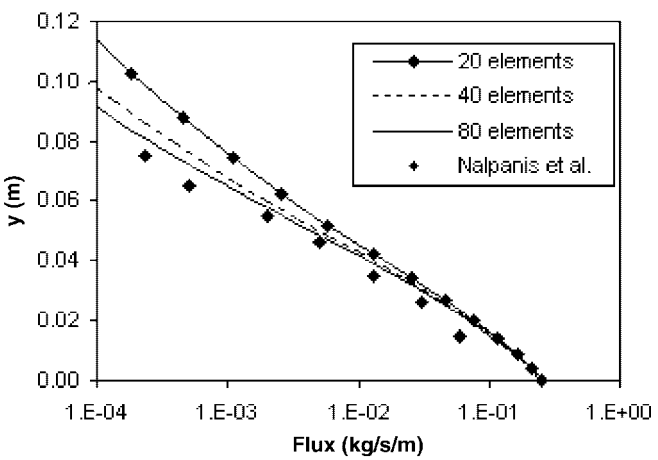

Figure 8. CFD grid sensitivity study of particle (sand) flux profile along a flat surface ($u_* = 0.35$, $d = 188$ μm) compared against the results of Nalpanis *et al.* [6].

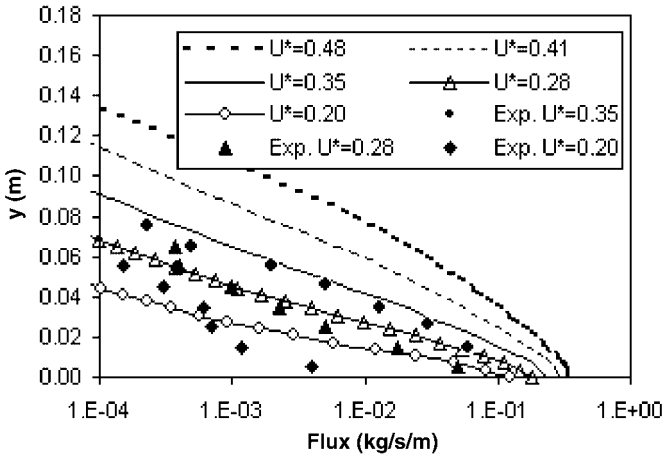

Figure 9. CFD predictions of particle (sand) flux profile along a flat surface compared against the results of Nalpanis *et al.* [6] at various shear velocities and average particle size of $d = 188\ \mu\text{m}$.

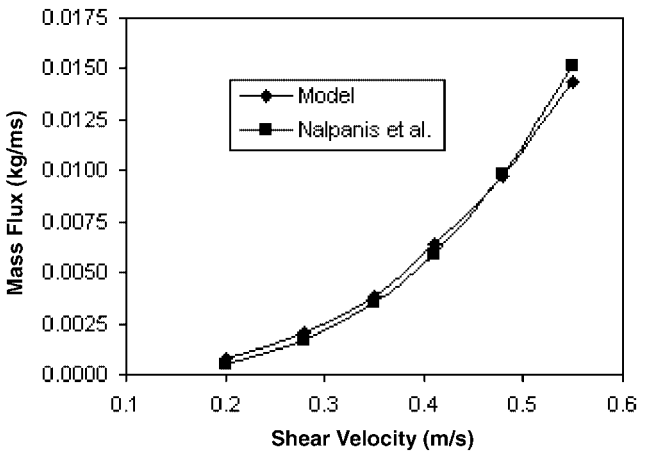

Figure 10. CFD predictions of total entrained particle flux over a flat surface compared against the results of Nalpanis *et al.* [6] at various shear velocities and average particle (sand) size of $d = 188\ \mu\text{m}$.

small compared to the total diffusivity coefficient (here given a value equal to the fluid dynamic viscosity). The turbulent diffusivity coefficient, Γ_t, is calculated using Equation (6) and the turbulent Prandtl number, σ_d, calculated with Equation (37). This coefficient decreases towards the surface, while the saltation diffusivity, Γ_s, has its maximum at the surface and gradually decreases to the top of saltation layer. The extent of the influence of Γ_s depends on the shear velocity, which in turn influences the saltation layer thickness as shown in Figure 12. The complexity of the saltation/suspension activity at the surface is now described

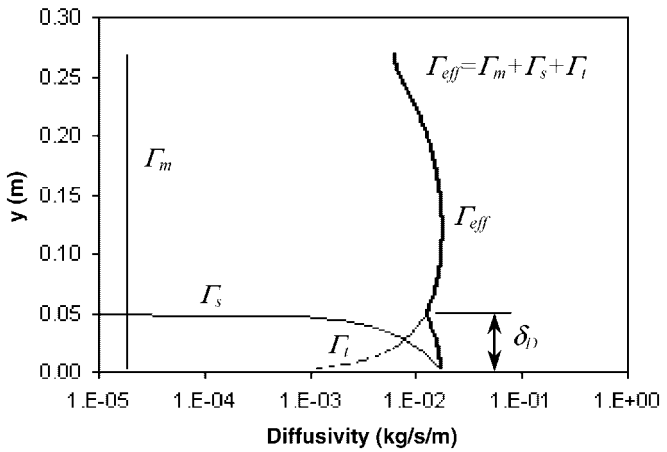

Figure 11. Effective turbulent diffusivity, and its components, for particle (sand) entrainment predictions at $u_* = 0.35$ and $d = 188\ \mu\text{m}$.

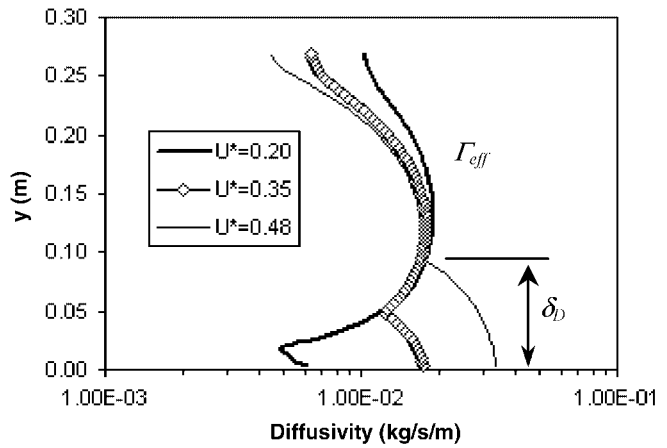

Figure 12. Effective turbulent diffusivity for particle (sand) entrainment at various shear velocities ($d = 188\ \mu\text{m}$).

in terms of an entrainment rate at the surface, settling fluxes through the algebraic slip terms in the governing particle transport equation, and a variable saltation diffusion coefficient scaled appropriately with the surface shear conditions. While shown for a simple duct geometry, it is proposed that this can be generalized to the cases where the near surface shear stress varies. The next example is intended to demonstrate such situations.

THREE-DIMENSIONAL FLOW EXAMPLE

To show the application of the method to more complex environmental flow conditions, experimental data for coal particles entrained from a box centred in a wind tunnel is applied [19]. The geometric conditions for the experiment are shown in Figure 13a, while the size-distribution for the coal particles is depicted in Figure 13b. The exposed surface area for each size class, as shown in Figure 13b, can be calculated from the mass fraction and average size class distribution. Obviously, the complexity of the coal surface requires some simplification, and for calculating the exposed surface area all particles (across all size classes) are assumed equally distributed at the surface, and the projected surface area calculated on a plane passing through the centre of all exposed particles. The top layer of particles are assumed continuously replenished. The entrainment fluxes for a given size class are multiplied by the area fraction when assembling boundary conditions in the CFD solution procedure. For example,

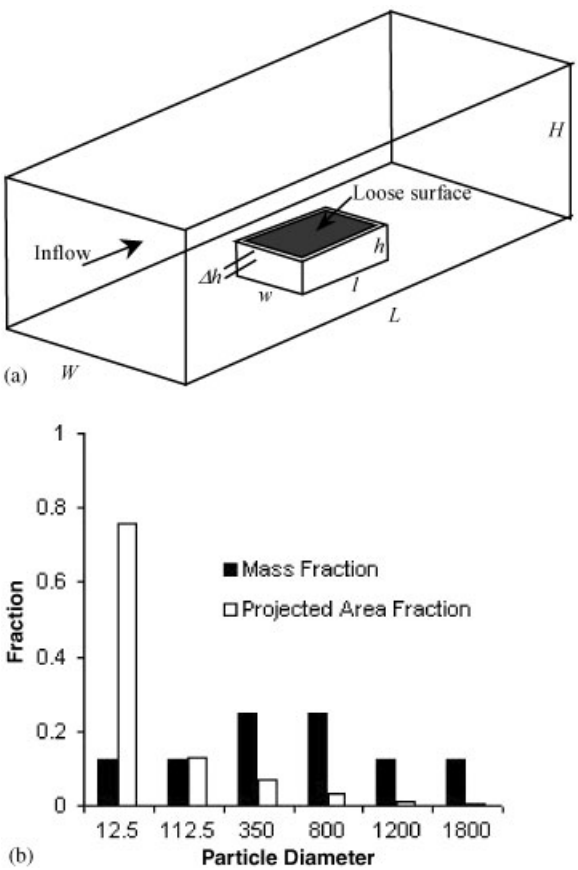

Figure 13. (a) Wind tunnel geometry for box filled with coal, (b) measured particle size distribution and estimated exposed surface area for each size class. Note that geometry is scaled with respect to actual coal car dimensions [19].

Equation (9) would be multiplied by a fraction of the total surface area when applied for a specific size class. For the geometry corresponding to the experiment, the parameters in Figure 13a are $h = 150$, $l = 432$ and $w = 99$ and $\delta h = 10$ mm. The last parameter is the initial depression of the coal surface from the top of the box, and is assumed fixed since surface deformations are not considered in this study.

The inlet velocity in the actual experiment was 13.4 m/s, and the corresponding weight of material removed from the box, with time, was measured. The total particle removal rate from the box, once past the initial start-up period, was observed to be nearly uniform for the test that ran for approximately 1.4 h. This quasi-steady response was then modelled as a steady-state process in CFD. In Plate 1 is shown features of the predicted steady-state results for this case. Along the coal surface the predicted shear stress distribution is shown, followed by the speed distribution just above the box and within the box. It is apparent that the flow is highly three-dimensional with strong variation in the surface conditions as indicated by the shear stress distribution. The model applied in the previous examples is now applied by assuming a local one-dimensional saltation behaviour. Also shown in Plate 1 is the predicted concentrations for the 12.5 and 350 μm particle sizes. The smallest particle sized can be readily removed from the surface and transported beyond the car into the free stream. The settling fluxes are small and the particles are transported out of the wind tunnel. However for the larger sizes fewer particles are removed from the box, and if they do, settle to the floor of the wind tunnel quickly. Solutions were also obtained for particle sizes 112.5 and 800 μm but not shown for the sake of brevity. The largest two particle sizes (see Figure 13b) were not solved since they do not leave the box due to their weight. In the CFD solution, equations for all of the particle classes are solved in conjunction with the hydrodynamic variables.

The overall predicted response of the surface, under wind action at free-stream velocity of 13.4 m/s, is shown in Figure 14. In Figure 14a the entrainment flux leaving the surface (Equation (9)) is shown for each size class, as well as the corresponding settling flux at the surface. The settling and entrainment flux become the same as particle size becomes larger, reflecting the difficulty in removing large particle sizes from the box. The net removal for a given size class is therefore also shown, and approaches zero for the larger size classes. The accumulated (integrated across all size classes) rate of material removal is also shown in Figure 14a and compared to the experimental value. Considering the complexity of the two-phase system, the correct order of magnitude is predicted. In Figure 14b, the response of the coal surface to variation in the free-stream velocity is shown. As expected at high velocities, and correspondingly higher levels of surface shear stress, more material is removed out of the box and into the free-stream.

It should be noted that in the actual experiment, a small deformation in the surface profile was observed due to particle removal and settling. The deformation, although present, was small enough to make the assumption of a non-deformable surface appropriate.

CONCLUSIONS

A practical modelling approach for including the influence of saltation and suspension along loose boundaries has been proposed. Utilizing the logarithmic and total entrained particle flux profiles observed in experiments, functional relationships, dependent on particle size and wall shear velocity only, have been derived for the near surface effective diffusion (Equation (24)),

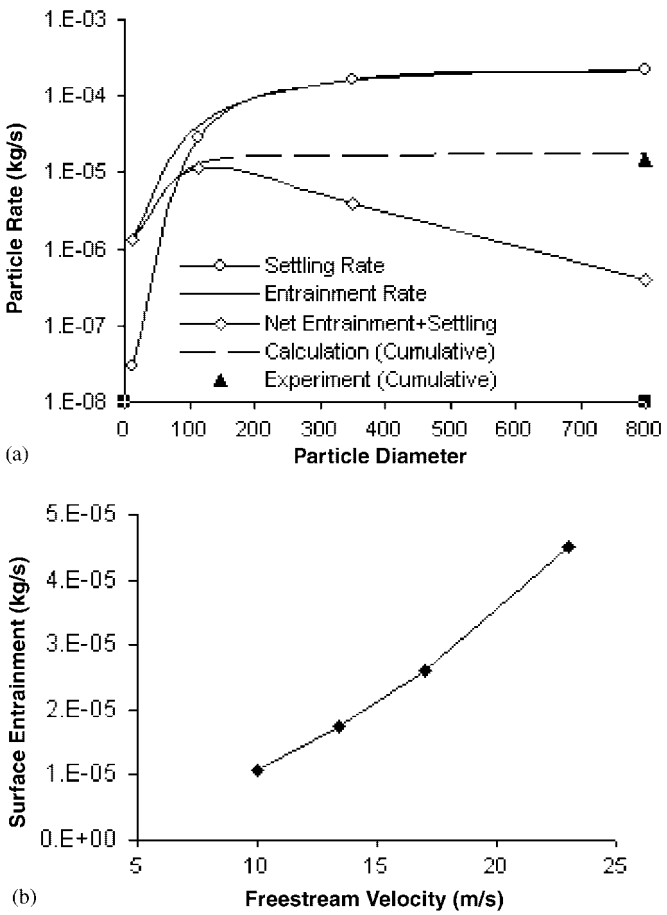

Figure 14. (a) Entrainment and settling rates (and their net) for each particle size class along with total accumulated rate of removal, and (b) total removal rate from the box as a function of free-stream velocity.

surface entrainment coefficient (Equation (30)), and saltation diffusion coefficient (Equation (38)). The last two equations can be employed in a CFD environment utilizing particle transport equations to predict the distribution of particles in dilute systems.

The computation results show a good agreement with both experimental and analytical results of Nalpanis *et al.* [6] and Anderson and Haff [3]. Importantly the total entrainment as a function of surface shear velocity is well predicted for a given particle size. The derived equations are applicable to a fixed particle size, however in the CFD solution n number of independent particle transport equations can be utilized to predict the distribution of n different particle sizes. To demonstrate this a three-dimensional solution of coal entrainment from a box in a wind tunnel was provided. The calculated results for one flow velocity are compared to experiment and show good agreement with the total rate of material removal across all size classes. The example also demonstrates the application of the derived equations, for estimating

the near surface saltation/sedimentation behaviour, to a case where local one-dimensional assumptions are made.

Future work will apply the CFD methodology to more general loose surface situations, including loose surfaces with a distribution of particle sizes. While the present model has been described in conjunction with a k–ε turbulence model, the method proposed will work in conjunction with any other RANS turbulence models since it depends only on the estimate of the effective turbulent viscosity.

NOMENCLATURE

C_D	drag coefficient
C_s	total mass flux coefficient
d	particle diameter (m)
$f(y)$	vertical particle flux profile
F	total horizontal particle flux (kg/(ms))
F_i	viscous stresses (N/m^2)
g	gravitational acceleration (m/s^2)
k_0	initial velocity factor
m_p	mass of particle (kg)
$\dot{m}_p$	particle mass flux (kg/(m^{2}s))
$\dot{N}_a$	particle entrainment flux (#/(sm^2))
Re_p	particulate Reynolds number
u	fluid velocity (m/s)
u_* or U^*	fluid shear velocity (m/s)
V_a	particle entrainment velocity (m/s)
V_e	particle ejection velocity (m/s)
V_r	particle rebound velocity (m/s)
V_s	particle impact velocity or settling velocity (m/s)

Greek

δ_D	average saltating height (m)
Γ_{eff}	effective diffusivity coefficient (kg/(ms))
Γ_m	molecular diffusivity coefficient (kg/(ms))
Γ_s	saltation diffusivity coefficient (kg/(ms))
μ	dynamic fluid viscosity (kg/(ms))
μ_t	turbulent viscosity (kg/(ms))
ϕ	loading ratio (kg/kg)
ρ	fluid density (kg/m^3)
ρ_p	particle density (kg/m^3)
σ_d	turbulent Prandtl number
τ_0	critical shear stress on the surface (N/m^2)
τ_w	wall shear stress (N/m^2)
ζ	entrainment coefficient (s/m^2)

ACKNOWLEDGEMENTS

The authors are grateful for the support received from the University of New Brunswick, and the Natural Sciences and Engineering Research Council of Canada (Discovery Grant—A.C.M. Sousa). The provision of experimental data by Dr. A.D. Ferreira from the University of Coimbra, Portugal, is much appreciated.

REFERENCES

1. Bagnold RA. *The Physics of Blown Sand and Desert Dunes*. Methuen: London, 1941.
2. Owen PR. Saltation of uniform grains in air. *Journal of Fluid Mechanics* 1964; **20**(2):225–242.
3. Anderson RS, Haff PK. Wind modification and bed response during saltation of sand in air. *Acta Mechanica* 1991; **1**(Suppl):21–51.
4. Anderson RS, Haff PK. Simulation of aeolian saltation. *Science* 1998; **241**:820–822.
5. Werner BT, Haff PK. The impact process in aeolian saltation: two dimensional simulations. *Sedimentology* 1988; **35**:189–196.
6. Nalpanis P, Hunt JCR, Barrett CF. Saltating particles over flat beds. *Journal of Fluid Mechanics* 1993; **251**: 661–685.
7. Nishimura K, Hunt JCR. Saltation and incipient suspension above a flat particle bed below a turbulent boundary layer. *Journal of Fluid Mechanics* 2000; **417**:77–102.
8. Sherman DJ, Jackson DWT, Namikas SL, Wang J. Wind-blown sand on beaches: an evolution of models. *Geomorphology* 1998; **22**:113–133.
9. Sherman DJ, Namikas SL. AEOLUS: an interactive program for the simulation of aeolian sedimentation. *Geomorphology* 1998; **22**:135–149.
10. Ni JR, Li ZS, Mendoza C. Vertical profiles of aeolian sand mass flux. *Geomorphology* 2002; **49**(3–4): 205–218.
11. Dong Z, Liu X, Wang H. The aerodynamic roughness with a blowing sand boundary layer (BSBL): a redefinition of the Owen effect. *Geophysical Research Letters* 2003; **30**(2):1047.
12. Ji S, Gerber AG, Sousa ACM. An efficient CFD model for air/particle saltating flows. *IMECE*-2002, November 17–22, New Orleans, USA, 2002, CD#32090.
13. Ushijima S. Arbitrary Lagrangian–Eulerian numerical prediction for local scour caused by turbulent flows. *Journal of Computational Physics* 1996; **125**:71–82.
14. Alhajraf S. Three-dimensional homogeneous two-phase flow modelling of drifting sand around an open gate. In *Computational Methods in Multiphase Flow*, Power H, Brebbia CA (eds). WIT Press: UK, 2001; 309–325.
15. Launder BE, Spalding DB. The numerical computation of turbulent flows. *Computer Methods in Applied Mechanics Engineering* 1974; **3**:269–289.
16. Raudkivi AJ. *Loose Boundary Hydraulics*. Pergamon Press: Oxford, 1976.
17. Schlichting H. *Boundary Layer Theory*. McGraw-Hill: New York, 1955.
18. Wilcox DC. *Turbulence Modeling for CFD* (2nd edn). DCW Industries, La Cañada, CA, 1998.
19. Ferreira AD, Vaz PA. Wind tunnel study of coal dust release from train wagons. *Journal of Wind Engineering and Industrial Aerodynamics* (in press).

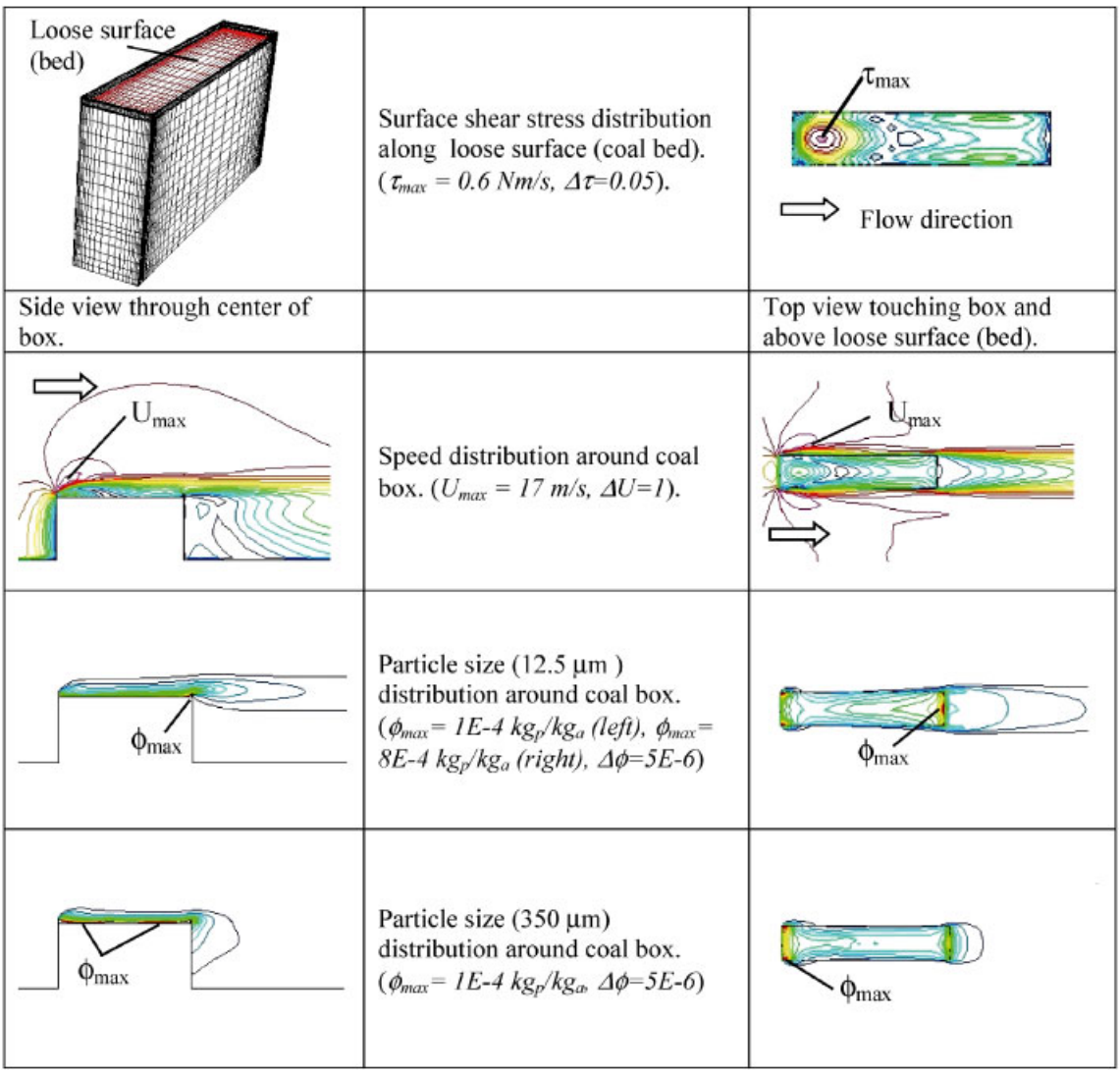

Plate 1. Gallery of predicted shear stress, speed and particle concentrations for a free-stream velocity of 13.4 m/s. Shear stress is shown along coal surface, speed and particle concentrations are shown on a horizontal plane just above box and on a vertical plane through the box centre.